



POLITECNICO  
MILANO 1863

DIPARTIMENTO DI MECCANICA



## On the Geometrical Accuracy of High Aspect Ratio Micromilled Pins

Parenti, Paolo; Pagani, Luca; Annoni, MASSIMILIANO PIETRO GIOVANNI; Colosimo, BIANCA MARIA; Semeraro, Quirico

This is a post-peer-review, pre-copyedit version of an article published in JOURNAL OF MANUFACTURING SCIENCE AND ENGINEERING, 139/5, on November 10, 2016. The final authenticated version is available online at: <http://dx.doi.org/10.1115/1.4035035>

<https://asmedigitalcollection.asme.org/manufacturingscience/article/doi/10.1115/1.4035035/377563/On-the-Geometrical-Accuracy-of-High-Aspect-Ratio>

This content is ASME © provided under [CC BY-NC-ND 4.0](https://creativecommons.org/licenses/by-nc-nd/4.0/) license



## **On the geometrical accuracy of high aspect ratio micromilled pins**

Parenti Paolo\*, Pagani Luca, Annoni Massimiliano, Colosimo Bianca Maria, Semeraro Quirico

Department of Mechanical Engineering, Politecnico di Milano, via La Masa 1, 20156, Milan, Italy

\*Corresponding author: [paolo.parenti@polimi.it](mailto:paolo.parenti@polimi.it), tel. +39 (0)2-2399-8530, fax. +39 (0)2-2399-8585

# On the geometrical accuracy of high aspect ratio micromilled pins

## Abstract

Geometrical accuracy of micro-features in micromilling is strictly related with the choice of cutting parameters. Their correct selection is a challenging task in particular when the target feature geometry is a high aspect ratio feature with tight tolerance requirements. Metallic micromilled pins are adopted in many different industrial applications as in the micromold technology field, in the microelectromechanical systems and in the biomedical devices and their geometrical accuracy represents a fundamental property for their functionality. This work outlines the connection between the achieved geometrical accuracy and the micromilling parameters and cutting strategies on pins with diameter = 100  $\mu\text{m}$  and height = 2 mm (i.e. Aspect Ratio = 20). Pin geometrical error features are extracted from 3D optical measurements and then correlated with cutting parameters to support machining process setup. A proper fitting based on *Chebyshev* functions is applied and a statistical analysis assesses the importance of each deviation component, in relation to the imposed cutting conditions. The proposed methodology fills the specific lack in the literature domain about micro-pin machining and can easily extend to different types of geometrical micro-features. Finally, correlation between part geometrical errors and machining forces is analyzed. Cutting force analysis is adopted in conventional machining for implementing online geometrical errors assessment or compensation methods. However, this study confirms that the applicability of this approach in high aspect ratio pin micromilling is prevented from the predominant scale-effects and the large part bending, that generates a low direct correlation between forces and part geometrical errors.

**Keywords:** Micromilling, Geometrical quality, ANOVA, Focus Variation microscope

# 1. Introduction

The ability to create small features such as pins, bars, ribs, thin walls and micro channels with accurate geometries and dimensions is crucial for several applications and products. In microinjection molding and microextrusion products, these features are often obtained on metallic mold masters and extrusion males enabling the production of complex final products with hollow profiles [1].

Mechanical micromachining is the most productive and effective method to deal with complex 3D geometries and thin features, but the achievable quality can be limited, if compared with other processes such as microEDM, due to the characteristics of the cutting mechanism. In micromilling the scale effect and the low rigidity of the micro-tools exacerbates the overall complexity [2],[3]. In addition, when dealing with highly compliant part features, micromilling process parameters should be carefully designed and cutting strategies have to be reconsidered to control the final geometrical accuracy.

Many advanced analysis methods have been proposed to cope with these difficulties and sets of rules for cutting parameters and strategies optimization have been developed. Most of these methods address only traditional milling and rely on the use of Finite Element Method (FEM) simulation. Huang et al. in [4] have developed a flexible thermo-mechanical model for error prediction in thin-wall workpiece machining including a cutting stability analysis to overcome regenerative chatter onset. Bolsunovskiy et al. [5] have used Finite-Element Modeling to study vibration arising during machining of thin-wallet part: a strategy to select the best cutting speed to avoid forced vibration of the part considering its time changing dynamic behavior due to material removal has been proposed. All these methods are generally validated using limited number of experiments on a limited set of geometries and their extension to different machining cases and fields, such as micromachining, are not discussed.

Thin pins are very critical since they are one of the less rigid machinable features and therefore are subjected to deformation and breakage due to the cutting forces. Only few studies dealing with micro pins milling can be found in literature and they mostly aim at demonstrating the process capability to machine high aspect ratio pins, without investigating the best machining conditions to obtain good quality pins. Pin quality definition itself lacks in the literature. The study of Bang et al. [6] describes the design and testing of a selfmade PC-based 5-axis micromilling machine that demonstrated to be able to machine several features, such as thin walls, micro impellers and micro blades and high aspect ratio pins (30  $\mu\text{m}$  diameter pins with a height of 650  $\mu\text{m}$ ,  $AR = 21.6$ ) on brass. The pins were machined by rotating them along their axis, hence using the milling machine as a lathe. However, the authors did not point out the relationship between process parameters and workpiece quality. Bordatchev et al. [7] used brass as target material

and machined pins with a maximum AR of 30 (diameter = 200  $\mu\text{m}$ ; height = 6 mm). No different process parameter sets were investigated and no detailed workpiece quality measurements were performed in this study.

Literature lacks in providing specific knowledge to select the process parameters in pin micromilling and to identify quality outcomes. There is therefore a need of systematic approaches dealing with relationships between process parameters and workpiece quality for supporting the machining of these kind of features. Previous study by the authors pointed out the process parameters effect on workpiece quality and cutting forces in case of thin wall manufacturing [8]. A similar approach is applied here, adding a more systematic method to analyze the results of the manufacturing process. The presented method, based on *Chebyshev* fitting applied on the cylindrical geometry, improves what the authors have presented in a previous paper [9], which adopted the independent error computation method.

Moreover, in presence of reduced stiffness of the workpiece and/or of the tool, cutting forces can be employed for indirect estimation of geometrical errors on the machined parts as demonstrated for different machining processes in literature: turning [10], milling [11] and grinding [12]. Once the cutting mechanism generates contact forces, a relative displacement between the tool and the part rises, leading to a modification of the actual tool engagement and consequently to a modification of the instantaneous removed material. A conjunct analysis of cutting forces and tool positions signals can therefore lead to estimate the geometrical errors on the machined parts and localize their positions. This interesting approach works for traditional macromilling operations of aerospace components as demonstrated in [11] where cutting process of thin walls is monitored through cutting forces leading to estimate part thickness deviations. Real-time acquisition of the cutting forces can be also exploited for optimizing micromilling process of thin walls, as discussed in [13]: this work focused the attention on the average cutting force value and on the use of static FEM analysis for obtaining valid models for the bending phenomenon of the machined micro-ribs. In general, the idea to exploit force measurement for online geometrical part assessment is of particular interest for micromilling where an online characterization of the part would permit to avoid the usual time-expensive post-process measures of the part geometries. Therefore, this paper presents the correlation analysis between cutting forces and geometrical deviations of high aspect ratio pins to verify the capacity of the force based approach for assessing the pin geometrical quality.

First, the paper introduces the selected part geometry and the experimental conditions followed by a brief analysis of the process kinematic that supports the selection of the cutting parameters. Pin measurement and extracted pin error

features are analyzed along with quantitative results. Eventually, the force analysis is provided followed by a final discussion regarding the achieved results.

## 2. Micromilling process analysis

This work has the main aim to develop parameters selection criteria in micromilling of thin pins, taking into account their final geometric accuracy. To turn the obtained results into a generalized knowledge usable in different situations, a methodological approach is designed. This paragraph introduce it describing the selected pin geometry and material, the adopted milling machine and the applied sensors and measurement devices.

When machining a micro part, many different factors affect the final geometric accuracy. When the part is characterized by low stiffness, cutting forces may create deflections comparable with the targeted feature, thus compromising the production process. For these reasons, to produce parts with good accuracy the very low cutting forces generated in micromilling have to be controlled finely by means of proper cutting parameters selection, A  $2^4$  factorial design, replicated three times, was adopted to investigate the effects on the final geometry of the pins. The design factors are the axial depth of cut  $a_p$ , the radial depth of cut  $a_e$ , the feed per tooth  $f_z$  and the *upmilling/downmilling* strategies (Table 1). Central points were added for all the continuous factors generating a total number of 60 runs. All the runs were completely randomized for confounding the effect of unmeasurable factors and disturbances (Appendix B). Moreover, a block factor was adopted on the tool: first 30 tests was carried out with tool unit #1 and second 30 tests with the tool unit #2 (both units was the same type).

**Table 1: Designed Experimental Plan**

<u>PARAMETER</u>		<u>Level -1</u>	<u>Level 0</u>	<u>Level +1</u>
<b>Axial depth of cut</b>	$a_p$ [mm]	0.066	0.133	0.2
<b>Radial depth of cut</b>	$a_e$ [mm]	0.2	0.5	0.8
<b>Feed per tooth</b>	$f_z$ [ $\mu\text{m}/\text{rev tooth}$ ]	12.5	18.5	24.5
<b>Strategy</b>		<i>upmilling</i>		<i>downmilling</i>

## 2.1. Workpiece material, cutting cycle and tools

The targeted geometrical feature is the above-mentioned cylindrical pin with AR equal to 20 (radius  $R_p = 50 \mu\text{m}$ , height = 2 mm) as depicted in Figure 1, made by a non-alloy quality Carbon steel (C40-EN 10277-2-2008) with hardness of 200HRB.

In industrial applications, pins can be found in a single or in a multiple configurations, depending on the different cases. When pin matrices are adopted, a reduced pin centre-to-centre distance may impose the need to use extremely fine end-mills, with reduced static stiffness, thus increasing the manufacturing challenges. This study focuses on the single pin configuration in order to avoid the constraints on the mill dimensions. Further studies are in progress on the multiple pin configuration case.

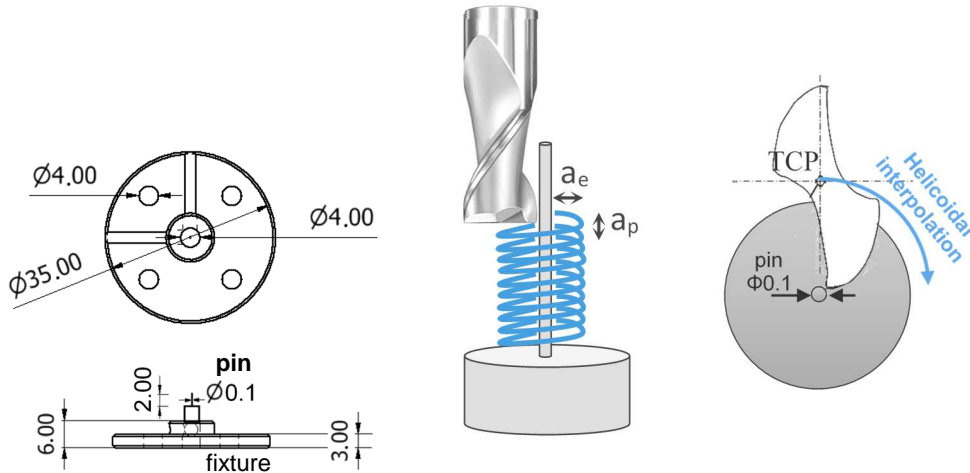
The manufacturing cycle consists of four phases. The raw cylindrical parts are obtained by turning 12 mm long and 4 mm wide bars, until a diameter of 2 mm is reached. A face milling operation of the top workpiece surface was carried out by means of a 6 mm diameter flat end mill to generate the reference plane that creates the total pins height. Afterwards, a roughing operation of the pins was performed with a Sandvik CoroMill Plura carbide end-mills (R216.32-02030-AC60P 1630) in a 2 mm diameter version in order to attain a precise final diameter of the roughed pin, according to the prescribed radial depth of cut  $a_e$  of the finishing operation. For instance when  $a_e=0.2$  mm was required for finishing, the pin diameter was set after roughing to have a diameter of 0.5 mm. In this way, the target pin diameter of 0.1 mm can be reached in one single finishing pass.

The adopted milling tool has 2 cutters, helix angle  $\theta_f=30^\circ$ , radial rake angle  $\gamma_r=10.5^\circ$ , axial rake angle  $\gamma_f=13.5^\circ$  and represents a standard choice for contouring, slot and square shoulder operations on steel parts. Finally, finishing operations were performed, with the same tool type used for roughing, according to the cutting parameters defined by the experimental plan design (Appendix B).

Tool wear is taken into account by foreseeing a tool change of the roughing tool after 30 tests (half of the total amount) and a block in the experimental plan, constituted by the tool unit, was therefore adopted. At the same time, a single finishing tool was used due to the very limited wear associated with the small material removed in this phase. Nevertheless, finishing tool is checked after the tests (total removal approximately equal to  $14 \text{ mm}^3$ ) showing negligible wear on either the rake and flank faces.

An interpolated toolpath generated with CAM software is used for finishing operations with a 3-Axis machine configuration. The tool engagement is imposed according to the runs of the experimental plan (Appendix B). The selected machining strategy is of helicoidal type: this strategy is suggested for pin micromilling because it leaves larger

stock on the part during pin cutting (i.e. during the rotations of the mill around the main pin axis). In the same way the step-support type does in thin-walls milling [8],[13], this limits the part deflection and the final geometric deviations on the part. The effects of different cutting strategies on the final part deviations will be carried out as a further development.



**Figure 1: Machined pin and fixture geometry (A), radial and axial engagement (B), top view trajectory (C)**

## 2.2. Cutting parameters selection

The cutting parameters used in the experimental plan are determined through a preliminary experimental campaign based both on the mill manufacturer guidelines and on kinematic considerations involving chip formation mechanism, as explained in this section.

The four parameters that are investigated are (Table 1):

- Axial depth of cut  $a_p$  (i.e. pitch of the helicoidal toolpath)
- Radial depth of cut  $a_e$
- Feed per tooth  $f_z$
- Milling strategy (*upmilling* / *downmilling*)

The cutting speed is fixed at the nominal value suggested by the mill manufacturer for the selected material (120 m/min). The preliminary experiments confirmed that chip formation and chip discharge are appropriate with this speed and that material does not stuck on the tool face avoiding any additional tool wear. The range selection for the depth of cuts is based on prior experience and on preliminary testing. Axial depth of cut  $a_p$  is varied significantly between 66  $\mu\text{m}$  and 200  $\mu\text{m}$  in order to examine the joint effect of the axial engagement of the tool and the pin deflection under cutting forces (that varies in magnitude and directions when changing  $a_p$ ). The selection of the radial immersion  $a_e$  is made in



a similar way: since radial stiffness of the pin varies exponentially with its diameter the adopted wide range of  $a_e$  (200 to 500  $\mu\text{m}$ ) is expected to generate different process response. In addition, the larger the  $a_e$ , the longer the contact angle and contact time between the tool and the pin: this causes less intermittent cutting on the part and potentially affects dynamic response of the part under cutting forces, thus giving this parameter a large potential on the final pins accuracy.

As the final pin geometrical quality is the feature to investigate, process parameters are varied only for finishing operation, while roughing operations are performed with constant parameters using a specific roughing tool.

The choice of the feed per tooth is fundamental in micromilling since it deals with the ploughing mechanism that appears due to the Minimum uncut Chip Thickness (*MCT*) effect [3]. In particular, when the actual chip thickness is lower than the cutting edge radius of the mill, cutting mechanism and chip formation are strongly affected. This phenomenon can never be completely avoided in micromilling but a proper selection of the feed rate value can limit it to the beginning (*upmilling*) or to the end (*downmilling*) of the angular tool engagement. For the adopted untreated Carbon Steel (C40), the *MCT* ranges between 20% and 35% of the cutting edge radius [14]. The edge radius of the adopted end-mill is quantified in 5  $\mu\text{m}$  by performing a direct tool measurement by means of a 3D optical microscope (paragraph 3.3).

Another effect is played by the tool geometrical runout that affects milling performance through the modification of the actual chip thickness [3]. An accurate measurement of the tool before cutting was done through an optical presetting system (Visual Tool setter Marposs VTS<sup>®</sup>): and the total dynamic runout resulted in 5  $\mu\text{m}$  for the adopted end-mills.

This value is comparable with the cutting edge radius and therefore its effect is expected to be minimized by selecting the proper feed per tooth as discussed later. This system allows accurate tool measurements at its running conditions including all dynamics effects due to the rotational speed. Only pressurized air at 5 bar, with no additional lubrication, was adopted for all the cutting tests since preliminary tests demonstrated that this method adequately support chip evacuation from the contact area, minimizing the risks of chip clogging and chip re-machining for the selected material. When milling tool moves along complex trajectories, as the implemented helicoidal type, process kinematic must be take into account for the calculation of the actual chip thickness as a function of the imposed feed: the following paragraph addresses this aspect.

### **2.3. Cutting process kinematic**

In presence of micromilled features the cutting parameters selection has to take into account several aspects related with the nominal chip thickness, the cutting forces and the adopted toolpath. Since in micromilling variations of the

nominal rake angle, ploughing and elastic material recovery rise up during cutting (due to the big cutting edge radius of the mills in comparison to chip thickness), process planning and process parameters selection have to be carefully designed. The application of a mechanistic approach to produce an estimation of the cutting forces can support this phase. The main shearing components of micromilling forces,  $F_t$  (tangential) and  $F_r$  (radial) can be represented by the following relationship:

$$F_t(\theta) = K_t(h_n, r) \cdot a_p \cdot h_n(\theta)$$

Eq. (1,2)

$$F_r(\theta) = K_r(h_n, r) \cdot a_p \cdot h_n(\theta)$$

where  $\theta$  represents the angular tool position and  $K_t$ ,  $K_r$  represent the cutting force coefficients which varies with the uncut chip thickness (main component) and with the cutting edge radius  $r$  (edge effect). For a chip thickness lower than the  $MCT$  these coefficients increase exponentially as to describe the reduced material removal produced by the ploughing regime in respect to the pure shearing cutting regime.

Consider a given tool with radius  $R_t$  and a final pin radius  $R_p$ . After a soft entry, the tool fully engages in both axial and radial directions with nominal parameters, as illustrated in Figure 2.

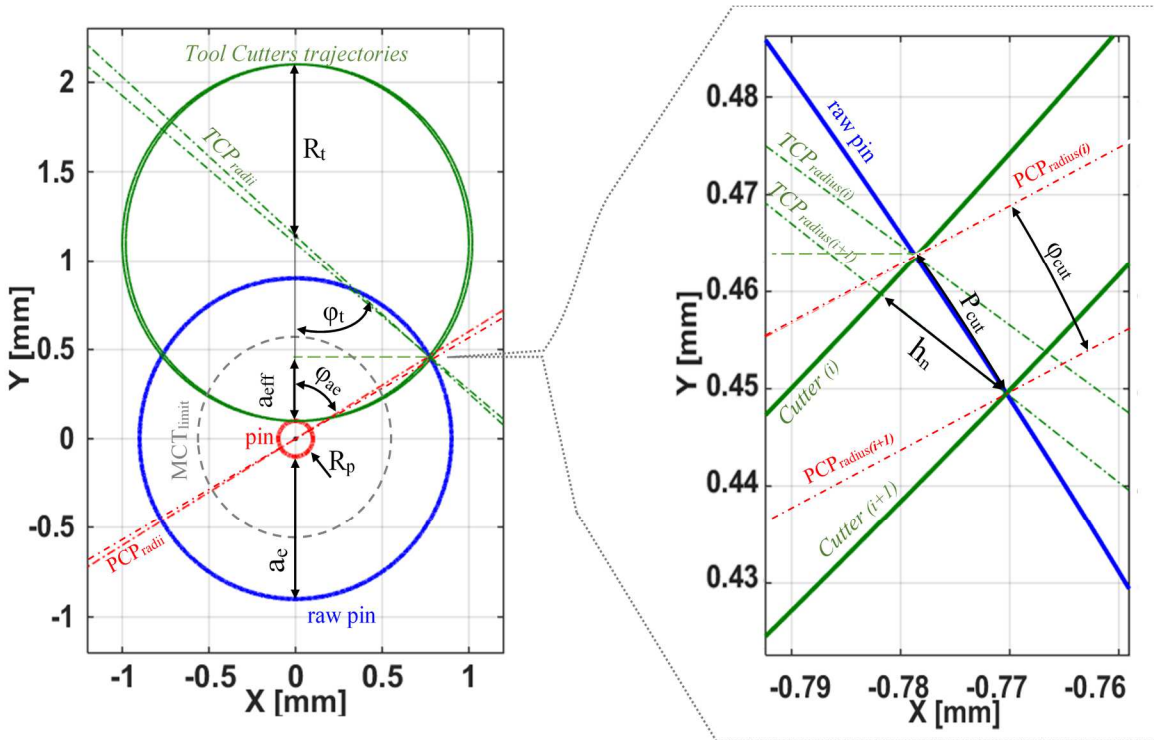


Figure 2: Tool engagement (A) top view, (B) detail of end contact point

The green dash-dot lines, connecting the Tool Center Point (*TCP*) and the contact point between each cutter trajectory and the raw pin, are indicated as *TCP radius(i)* and *TCP radius(i+1)*, for the first and the second cutter, respectively. The same connecting lines are in red for the Pin Center Point (*PCP*) and are indicated as *PCPradius(i)* and *PCPradius(i+1)*, respectively. The circular trajectories of the two cutters are indicated with a green solid line. The tool trajectory is such that chip thickness is zero when approaching the final pin surface and increases during rotation, reaching the maximum thickness imposed by the adopted feed per tooth. Consequently, a ploughing-dominated cutting area can be identified with the grey dash line (*MCTlimit*) in Figure 2. Basing on the modeling equations presented in Appendix A, the feed per tooth is set in the tests (Table 1), at least 2.5 times greater than the tool edge radius trying to limit ploughing area and the maximum force level. The selected trade-off value leads to a minimum extension of the *MCT* area at approximately 60% of the total contact arc. Further considerations related to *MCT* effect are discussed in chapter 4.

### 3. Experimental setup

#### 3.1. Machining center

Machining very thin parts with high aspect ratios requires extremely precise machines to limit the effect of volumetric machine errors that affect final part accuracy. Several reasons make the use of a high-end machining center mandatory for this manufacturing task. Miniature helicoidal trajectory requires a very precise and repeatable motion axes to assure the correct positioning of the tool during cutting but also very high linear speed and acceleration on the machine feed drives. This is because of the adopted circular trajectory of the tool around the pin that asks for sinusoidal laws on each machine axis. In this regard, machine rigidity has to tackle the high inertial forces during the acceleration phases to avoid tool tip deflections. Since axes undergoes periodic inversions during the interpolation, reducing the friction on the machine guideways is extremely important because it may lead to relevant motion errors and consequent geometric part deviations.

For these reasons, an ultra-precision 5-axis machining center (Kern EVO) with nominal positioning tolerance equal to  $\pm 1 \mu\text{m}$  is exploited for the cutting tests.

A properly designed fixture with two grains in X and Y direction is clamped on machine table to hold the workpiece during milling (Figure 1).

To support the achievement of high geometrical accuracy a touch probe (repeatability  $2\sigma < 1 \mu\text{m}$ , accuracy  $\pm 2 \mu\text{m}$ ) is used to read the workpiece position and define the reference system adopted in the machining cycle.

Eventually, the actual positions of the three machine axes during the cutting are logged every 1.8 ms through the machine numerical control (Heidenhain iTNC530) connected to an external PC via ethernet connection.

### **3.2. Cutting force measurement**

The implementation of effective process monitoring on the machine is essential to support the production of good micromilled parts. In general, cutting process monitoring can be based on accelerometers, microphones, AE sensors, forces and torque sensors or current sensors [3] whose information can be transformed into synthetic indications for online diagnostic during machining process. However, in case of micromilling only very sensitive and high bandwidth sensors can be employed due to the low system perturbation generated by the cutting [15].

Since this study focuses on geometric deviations of the pins, a dynamometer is adopted as a monitoring sensor in order to verify if the acquired cutting forces could provide useful information for the online prediction of these errors. A triaxial piezoelectric load cell is adopted (Kistler 9317B; linearity error  $\leq 0.5\%$  FSO, Full Scale Output, amplified by Kistler 5015A charge amplifiers and acquired by a National Instrument USB 6210 board at a 12000 Hz sampling frequency). A preliminary experimental verification studied the measurement error due to the bending moment generated by the cutting force and the results confirmed a good reliability of the force sensor setup.

Moreover, the high rotational speed required for small milling tools generates high frequency cutting harmonics that excite the dynamometer dynamic, corrupting the force measurement. Therefore, a dynamic compensation scheme is required to eliminate the introduced inertial effects. Results of the compensated forces acquisition are illustrated in chapter 5.

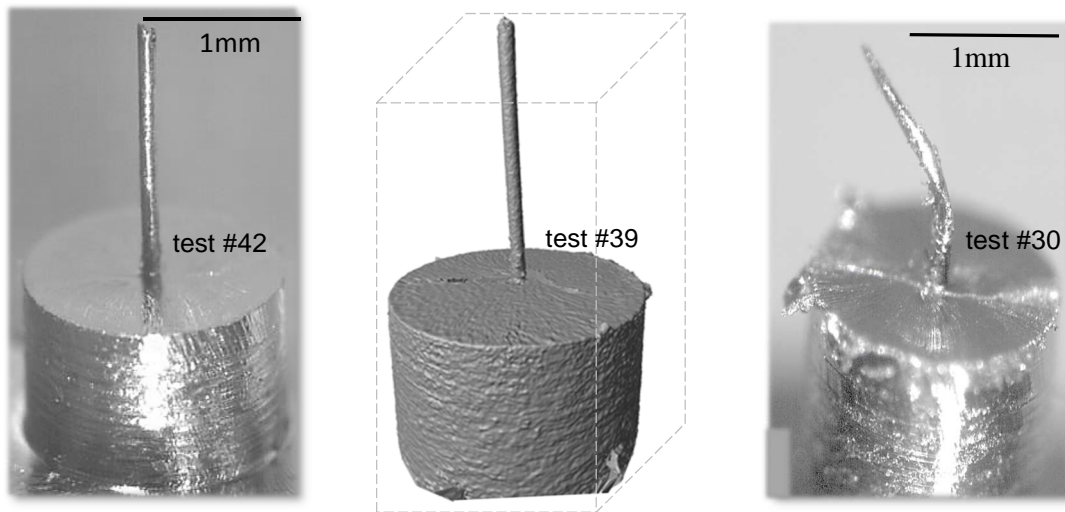
### **3.3. Pin geometry measurements**

Geometrical characterization of very tiny features with micrometric accuracy represents a hard task. A contact measurement device is not suitable because the generated contact forces introduce invalidating part deflections and high risk of part breakage. Among non-contact devices, traditional laser gauges can be adopted for capturing the pin height and diameter whilst a 3D measurement device is needed to compute a complete geometric characterization with high accuracy and repeatability: a 3D focus variation microscope is adopted in this study ( Alicona Infinite Focus ®). Despite the instruments accuracy was not classified for this specific measuring task, the declared precision is

under 1  $\mu\text{m}$  which is sufficient for the study. The good optical response of the workpiece surface simplified the light condition setup. An overall number of 40000 points were obtained as point cloud for each pin, with a 20X magnification lens and vertical resolution equal to 0.1  $\mu\text{m}$ . Each measurement run was time-consuming since it required around 4 hours to be completed.

#### **4. Analysis of the experimental data**

The data obtained from the experimental campaign are analyzed. The first relevant finding is that *upmilling* strategy resulted not suitable for machining the pins. All runs performed by that strategy (i.e. 30 tests) caused out-of-control pin geometries with collapse and breakage of the part (Figure 3). Pin collapse occurred randomly along the toolpath for the broken pins and no systematic behaviors was observed with the variation of cutting parameters. As well-known, *upmilling* and *downmilling* configurations generate different cutting mechanisms and the use of flexible tools on flexible parts exacerbate these differences. In these situations, overcutting (*upmilling*) or undercutting (*downmilling*) establishes, due to the deflection created by the cutting forces [3] but in *upmilling*, the strong ploughing occurring at the beginning of the engagement generates large cutting forces that worsen the situation causing additional deflection. In presence of an extreme static compliance of the part in radial directions, such as the pins, unstable and uncontrollable behaviors can therefore appear. Predicting these effects is all but simple. To predict the pin static instability one would have to take into account either the elasto-plastic structural behavior of the part and the elastic flexibility of the tool, together with the additional phenomena that arise due the coupling between these two aspects (i.e. forced vibration, regenerative chatter). As far as the authors know, no closed solutions have been presented so far in literature for these a complex cases and no further analysis are proposed in this paper to explain the broken pins, as results of the *upmilling* tests.



**Figure 3: Machined pins and 3D point cloud acquired by Focus Variation microscope (A: real pin test #42; B: microscope acquisition of test #39, C: real pin of test #30)**

#### **4.1. Geometrical analysis through data cloud processing**

Starting from the measured 3D point clouds, the geometrical analysis of the pin is computed. This paragraph describes the implemented methodology for the geometrical characterization. The C++ library Point Cloud Library (PCL) [16], in particular the *RANdom Sample Consensus* (RANSAC) algorithm [17], and the *Eigen library* [18] are exploited for all the computations.

From the measurements, the first result consists in the presence nearby the extreme pin zones of irregular burrs (top) and surface striations (bottom) (Figure 3). Those small irregularities affect the repeatability of the measurement process, without being relevant for the pins geometry, so that the cylinder is truncated to remove them from the analysis.

To perform the truncation, the pin base plane is defined by applying a robust least square fitting to the 2 mm cylinder from which the pin rises and therefore the *Main Cartesian Coordinate System* (MCCS) is defined (Figure 4).

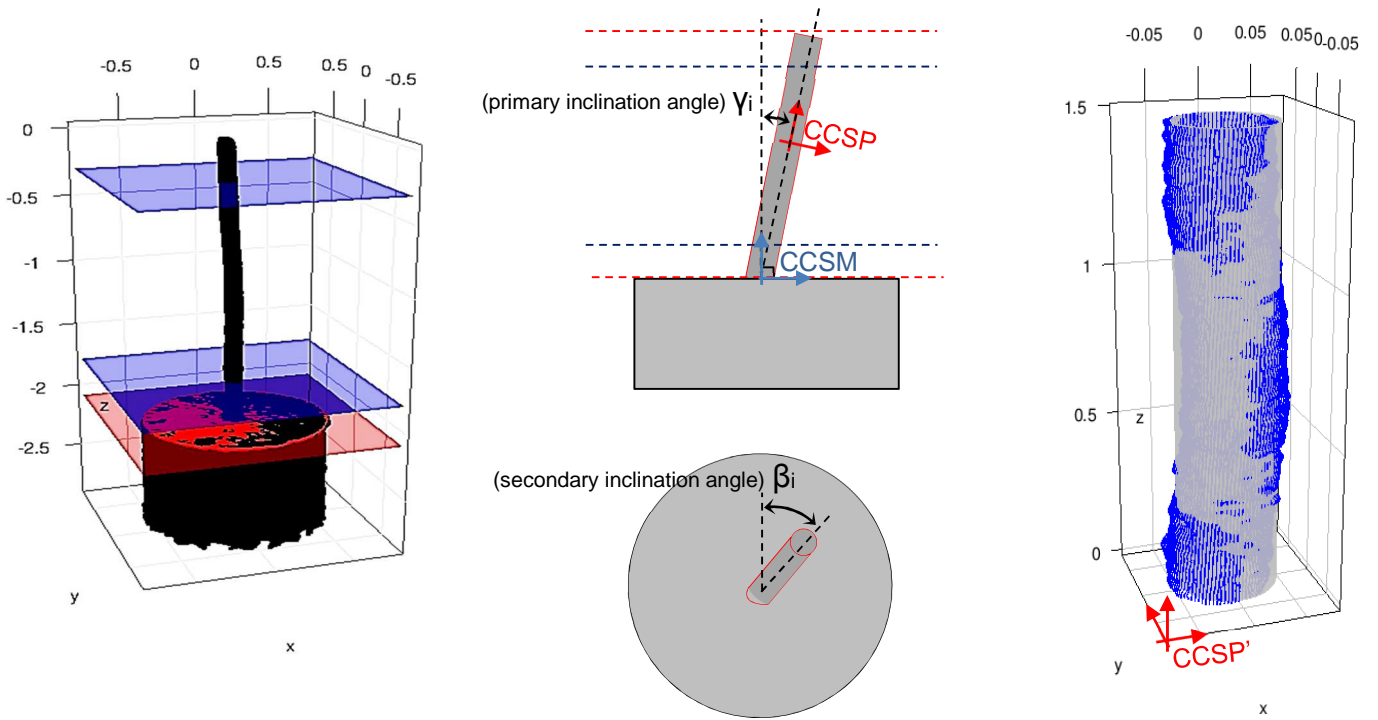
The points that lie on the top plane of the fitting cylinder constitutes the pin base, whilst the outliers are automatically filtered. The highest pin coordinate in Z direction, that determines the total pin height, is computed by shifting the base plane along the vertical coordinate of the main frame until cloud points statistically belong to that plane. Once the base and the top of the pin are defined, the initial and final pin parts are removed from the data cloud: a threshold of 0.3 mm is considered for both the upper and the lower bounds, as depicted in Figure 4. Then, a least-square cylinder is

computed and a related reference *Pin Cartesian Coordinate System (CCSP)* is defined by considering the axis of the *least-square cylinder (LSC)* as a reference *Z*-axis. The *LSC* diameter indicated with  $D_p$ , is used as reference to represent the pin diameter and is used to compute the diameter absolute error  $\Delta D_{err_{avg}}$  defined as:

$$\Delta D_{err_{avg}} = D_{nom} - D_p \quad \text{Eq. (3)}$$

where  $D_{nom}$  represents the pin nominal diameter, which is equal to 100  $\mu\text{m}$ .

At the same time, the orientation angular errors of the pin can be analyzed. The primary inclination angle  $\gamma_i$  is defined as the angular deviations of the  $Z_{CCSP}$  axis in respect to  $Z_{CCSM}$  axis on the *X-Z* plane. The other angular deviation of the  $Z_{CCSP}$  axis in the *X-Y* plane is defined as the secondary inclination angle  $\beta_i$ . All the following computation are based on the *CCSP'* plane, as depicted in Figure 4.



**Figure 4: Pin truncation planes (A), inclination angles definition (B) and Least squares cylinder-grey approximating the pin cloud-blue (C)**

#### 4.1.1. Inclination errors analysis

The orientation angle of the pin in respect to the base is of relevant importance for the pin functionality, especially when used as a mold core. To address this importance, the primary angle error  $\gamma_i$  (Figure 4) is studied. On the other

side, the secondary angle error  $\beta_i$  is not included in the analysis for preserving machine setup simplicity. To perform the microscope measurement of this angle, additional angular references in the milling setup would have been adopted to maintain the angular orientation of the pin during its detachment from the machine fixture, without being particularly useful for the final classification of the pin geometry.

Indeed, the primary angle error  $\gamma_i$ , can be easily extracted from the microscope measurement since the pin base gives the reference plane and the following analysis classifies the machined pin on the base of it. In this regard, a hierarchical clustering [19] is performed to check whether the pins can be clustered. Pins are grouped according to the Ward distance that minimizes the standard deviation between each cluster. According to the dendrogram showed in Figure 5, it is possible to set the number of the clusters to three (the red rectangles define the clusters). In this diagram, the abscissa includes the block value for each pin number. All the pins of the first cluster belong to the second block. This group represents the pin with the higher value of the angle  $\gamma_i$ . In the second group, all the pins except one, come from the first block: they show the minimal angular error and therefore the best machining performances. In the third group, the pins are coming from both the first and the second block.

The preliminary analysis shown that the goodness of the results depends on the block factor i.e. on the milling tool used for roughing operations. This fact confirms that the achievement of good geometric precisions on extremely flexible parts, such as high aspect ratio pins, cannot rely only on the setup of finishing cutting phase.

Since two identical tool units were used for roughing operations, their different effects on the pin inclination angle error  $\gamma_i$  is clear but remains somehow unexplained, with the measurements carried out in this experimentation. Further investigations need to be foreseen to deepen this aspect.

An *ANalysis Of VAriance* (ANOVA) [20] on the inclination angle  $\gamma_i$  is performed. The plots depicted in Table 2 and the coefficients p-values on Table 3 confirm that the block factor affects the primary angle at 95% of confidence interval. The factor  $f_z$  resulted significant as well. Among the interactions, only those between  $a_p$  and  $a_e$  and between  $a_e$  and  $f_z$ , seem to affect the result.



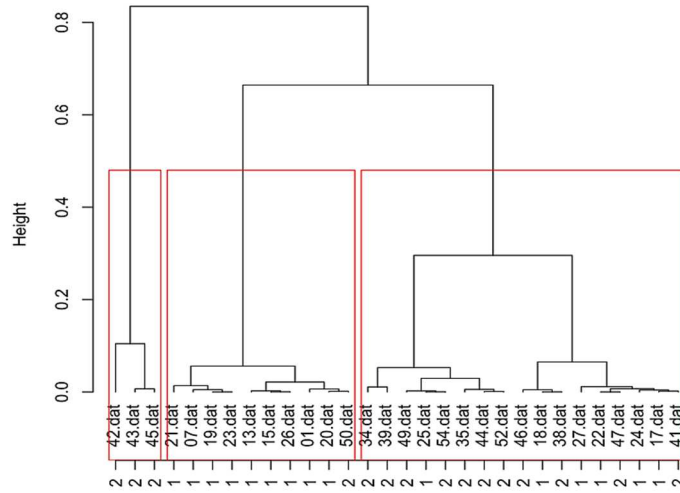


Figure 5: Cluster Dendograms of the main angle  $\gamma_i$  - Main Effect Plot of all the *downmilling* tests

Table 2: Plot Analysis for Cluster Dendograms

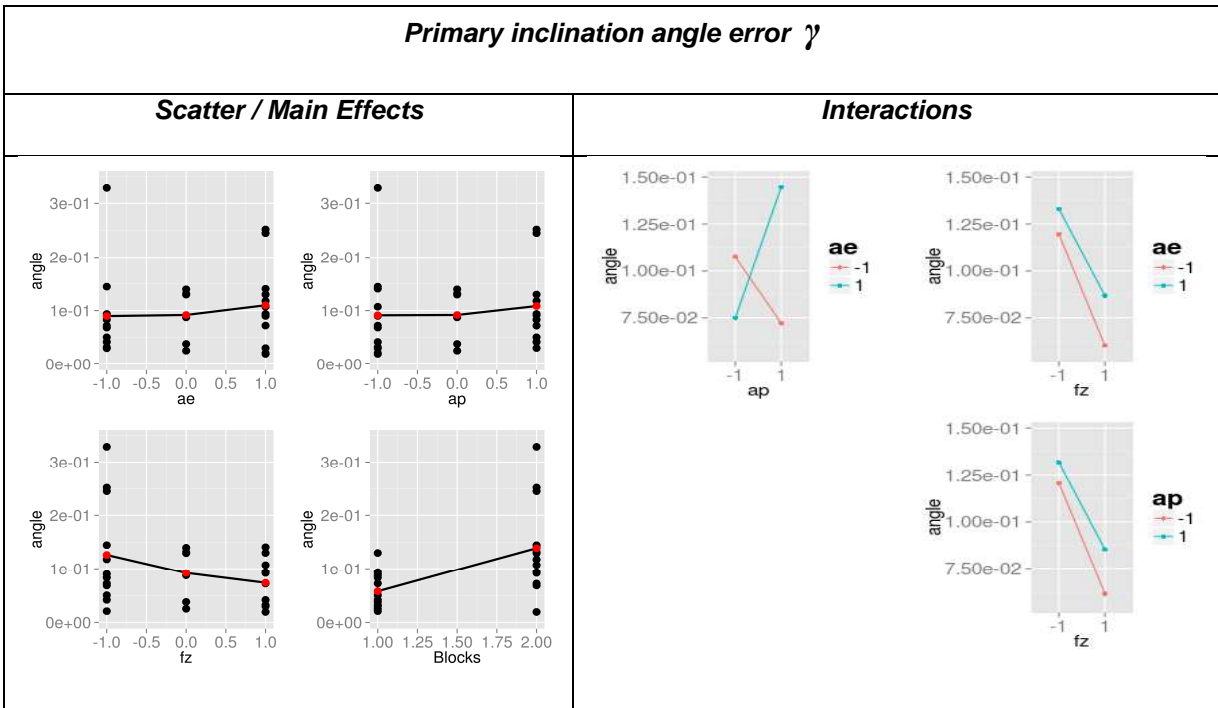


Table 3: ANOVA table of the main angle  $\gamma_i$

<b>Main Factors</b>			<b>Factors Interaction</b>			
$a_e$	$a_p$	$f_z$	$a_e a_p$	$a_e f_z$	$a_p f_z$	Block
0.381	0.451	0.028	0.029	0.029	0.773	<0.001

### 4.1.2. Shape errors modelling

Being able to classify the machining errors and to relate them with the causes that lead to their formation, assume a relevant importance for the machining operators and for the development of the related optimization strategies, as discussed by the authors in [21]. For the analyzed geometry, three different errors have been introduced above, namely the average pin diameter deviation, the primary and secondary inclination angles. However, other errors such as the cylindricity errors i.e. out of straightness, roundness or taper errors characterize the produced pins and they have to be extracted from the measured point clouds [22]. Different methods can be adopted for this purpose [23]. In a previous paper [9] the authors used the diameter absolute error, the taper ratio and the axis out of straightness as quality characteristics of the pin cylindrical geometry and each value was computed independently. In this work, the model is improved by adopting the approach that consider independent geometrical error shapes, as proposed in [24]. The adopted analytical method is based on *Chebyshev/Fourier* functions and assure good generality and performance over a wide range of manufactured products especially in case of 2.5D smoothed features. The method is suitable for creating the connection between the single and independent geometrical errors on the products and the original manufacturing process adopted. In this approach, *Chebyshev* functions are used to model the form error in the axial direction  $z$  while *Fourier* functions models the errors in the radial X-Y directions.

Let the actual geometrical deviations of the pin be described by the following equation:

$$R_{eff}(\theta, z_{norm}) = \frac{D_p}{2} + \Delta R(\theta, z_{norm}) = \frac{D_p}{2} + \sum_{l=0}^{N_v} a_{0l} T_l(z_{norm}) + \sum_{p=0}^{N_s} \sum_{l=0}^{N_v} a_{pl} T_l(z_{norm}) \cdot \cos(i\theta) + b_{pl} T_l(z_{norm}) \cdot \sin(i\theta) \quad \text{Eq. (4)}$$

where  $R_{eff}(\theta, z)$  is the actual radius of the part varying with the angular coordinate  $\theta$  and with the normalized vertical quote  $z$ ,  $\Delta R(\theta, z)$  is the radius deviations at the same coordinates,  $T_l(z)$  is the *Chebyshev* polynomials of second type (with order  $l$ ),  $a$ ,  $b$  are the *Fourier* Series coefficients,  $N_v$  and  $N_s$  are the selected total orders for *Chebyshev* and *Fourier* functions, respectively.

The polynomials are defined using a normalized interval ( $-1 \leq z \leq 1$ ) where the outer values corresponds to the pin ends ( $z = -1$  is the base while  $z = 1$  is the top). The normalized coordinate  $z_{norm}$  can be calculated as follows:

$$z_{norm} = \frac{2(z - z_{min}) - (z_{max} - z_{min})}{(z_{max} - z_{min})} \quad \text{Eq. (5)}$$

The functional  $T_l(z)$  is completely independent, i.e. orthogonal, to the z-axis coordinate  $z$  in the same way the *Fourier* terms are orthogonal to the angular coordinate  $\theta$ .

The resulting terms, describing each geometrical deviation shape, can be correlated directly to the cutting parameters, generating a useful technological feedback to the machining operators as a support for process control.

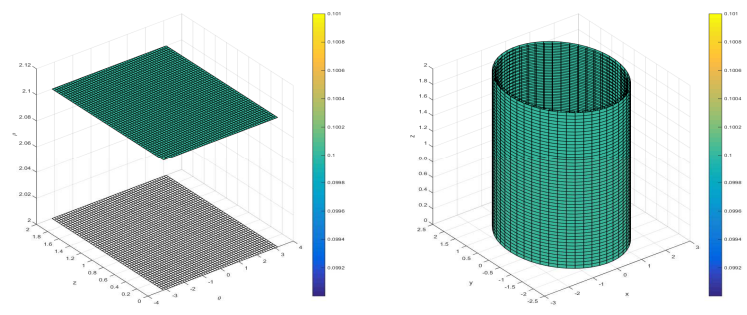
Preliminary cutting tests executed on the pin geometry confirmed that the axial geometrical deviations along  $z$  direction are much more relevant than those relying on the cross-sectional plane X-Y and therefore the *Fourier* terms are not included in the analysis.

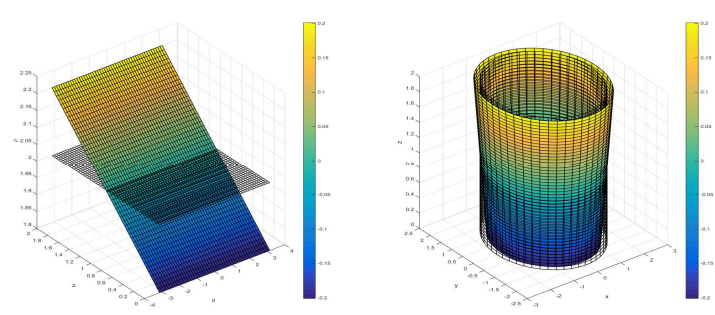
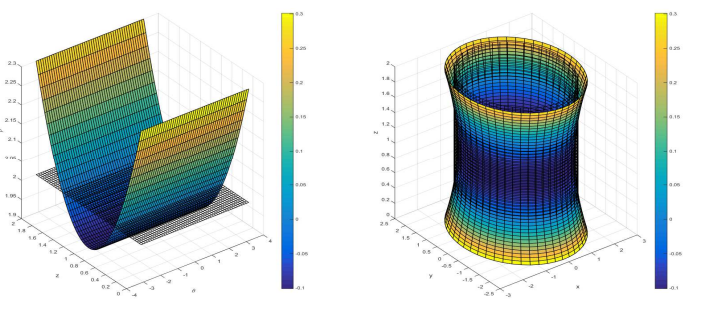
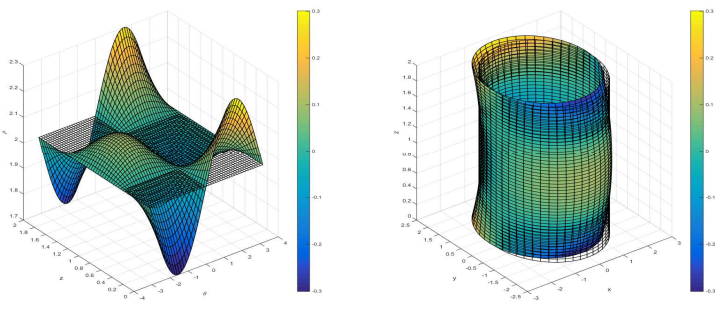
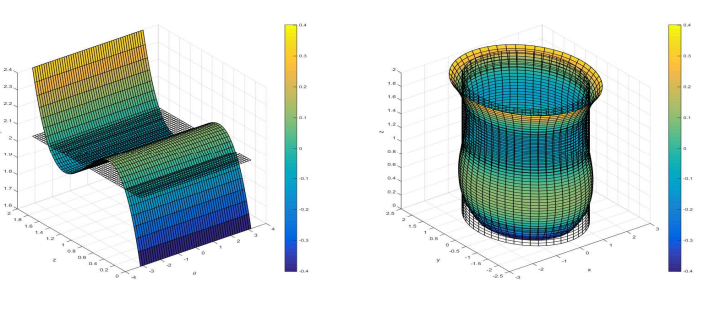
The systematic manufacturing errors of the micro-pins geometry are properly described by each terms of the analytical function. In this approach using the *Chebyshev* polynomials, the relation between the terms and the shape of the profile errors can be illustrated graphically (Table 4).

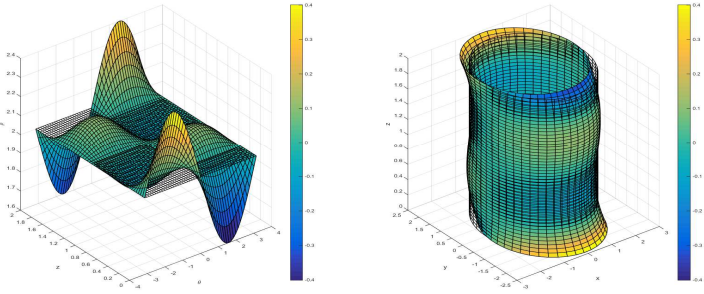
One good criterion for the choice of the function order is to increase the order until no statistical significance of the fitted terms appears. This analysis was carried out for the most representative pins finding that the first three terms ( $N_v=4$ ) are enough for describing the relevant geometric deviations.

Figure 6 depicts the fitting geometry on two experimental cases characterized by different error shapes (test #1, #45).

**Table 4: *Chebyshev* terms and related error shapes**

Type	Description	Order and Shape
<b>Diameter Scale</b> (same as $\Delta Derr_{avg}$ in Eq. 3)	Increment / decrement of actual diameter in respect to nominal value	$T_0(z_{norm})$ 
Type	Description	Order and Shape

<p><b>Taper</b></p>	<p>Monotonous variation of the radius along the vertical axis z</p>	<p style="text-align: center;"><math>T_1(z_{norm})</math></p> 
<p><b>Hourglass</b></p>	<p>Radius is lower (or higher) at the base and the pin tip whilst it is maximum (or minimum) at the center</p>	<p style="text-align: center;"><math>T_2(z_{norm})</math></p> 
<p><b>Banana</b></p>	<p>Radius is almost constant along z but the center of each X-Y slice deviates with the quote z</p>	<p style="text-align: center;"><math>T_2(z_{norm}) \cdot \sin(\theta)</math></p> 
<p><b>Bell</b></p>	<p>Radius changes according to a third degree polynomial, the upper and lower parts of the cylinder is bigger and smaller, respectively</p>	<p style="text-align: center;"><math>T_3(z_{norm})</math></p> 
<p><b>Type</b></p>	<p><b>Description</b></p>	<p><b>Order and Shape</b></p>

<p><b>S-shape</b></p>	<p>Radius is almost constant along z, but the cylinder axis has a S shape</p>	<p style="text-align: center;"><math>T_3(z_{norm}) \cdot \sin(\theta)</math></p> 
-----------------------	---	---

#### 4.1.2.1. Cutting parameters effects

The thirty *downmilling* runs and the related three factors complete model ( $a_p$ ,  $a_e$  and  $f_z$ ) are analyzed with an ANOVA. Table 5 summarizes the main results in terms of p-values of each geometrical quality characteristic (i.e. *Chebyshev* terms). In Table 6 the scatter and the effect plots are depicted for the  $T_0$  and  $T_1$  component. Since the test of the homogeneity of variance fails due to the within variability, a weighted least square approach is used. A weight equal to the inverse of the variance of each combination of the factor is chosen. First, as easily noticeable, the achieved pin diameter is most of the times bigger than the nominal one (Table 6). According to Table 5 the factors that more affect the coefficients  $T_0$ , representing the diameter variation, are  $a_p$  and the block. In particular,  $T_0$  increase as  $a_p$  increases. The higher forces produced by higher  $a_p$  certainly causes larger pin deflections generating a lower effective  $a_e$  with consequent higher local diameters. This consideration is supported by observing that  $a_e$ ,  $a_p$  and the mutual interaction between these two factors mostly affect the taper error, represented by the  $T_1$  coefficient. In particular,  $T_1$  decreases as  $a_e$  increases confirming the structural stiffening effect at the finishing pass caused by having more support to the pin on the opposite side of the mill. Lastly, another significant effect on  $T_1$  is caused by the block factor and by the interaction of  $a_p$  with  $f_z$ : with increased  $a_p$ , a further increase of  $f_z$  negatively affects the taper error whilst for reduced  $a_p$ ,  $f_z$  reduces it.

All these facts, confirm that local diameter variations are mostly lead by the flexural rigidity of the raw pin in conjunction with the nominal cutter engagement.

Summing up, to find the best value of the taper the interactions between the factors must be taken into account. In general, the effect of  $f_z$  on the analyzed geometrical deviations is less pronounced than the other parameters. This fact must be put in relation with to the minimum chip thickness effect that leads to an increase of the thrust forces acting on the pin proportional to the effective axial engagement of the mill.

The Barrel/Hourglass effect ( $T_2$ ) is due to  $a_e$  and its interaction with  $a_p$ , while the banana effect ( $T_2 \cdot \sin(\theta)$ ) is due to two factor interactions,  $a_e$  with  $a_p$  and  $a_e$  with  $f_z$  and the roughing milling tool adopted. The bell effect ( $T_3$ ) is determined by the value of the coefficients  $a_p$ , while the S-shape ( $T_3 \cdot \sin(\theta)$ ) is due to the factor  $f_z$ , its interaction with  $a_p$  and the value of the block factor.

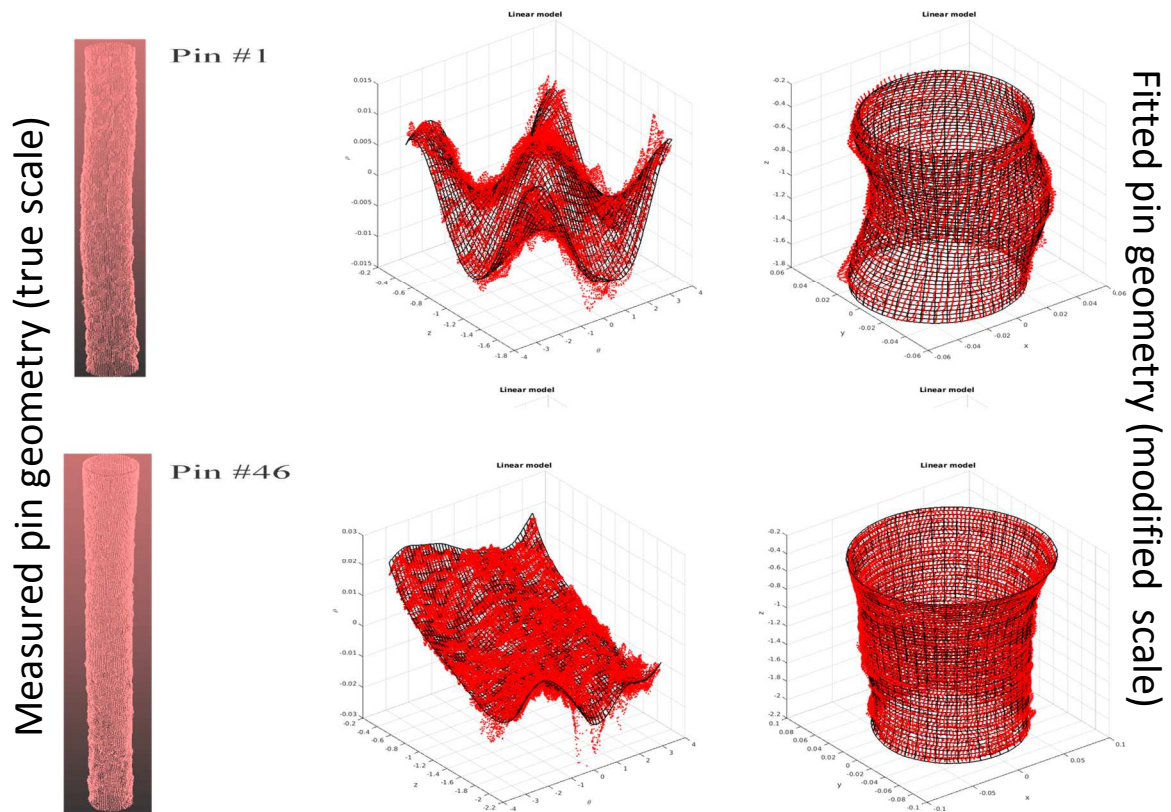


Figure 6: Chebyshev fitting on pin #1 (A), pin #46 (B)

Table 5: ANOVA results of the geometrical error shapes

Order	Main Factors			Factors Interaction			
	$a_e$	$a_p$	$f_z$	$a_e a_p$	$a_e f_z$	$a_p f_z$	Block
$T_0(z_{norm})$	0.38759	<0.001	0.070	0.503	0.126	0.554	<0.001
$T_1(z_{norm})$	<0.001	0.008	0.956	0.002	0.967	0.007	0.009
$T_2(z_{norm})$	0.004	0.036	0.457	0.006	0.466	0.029	0.020
$T_2(z_{norm}) \cdot \sin(\theta)$	0.038	0.488	0.085	0.002	0.002	0.054	0.002

$T_3(z_{norm})$	0.919	0.001	0.465	0.548	0.167	0.944	0.047
$T_3(z_{norm}) \cdot \sin(\theta)$	0.740	0.765	0.039	0.915	0.090	0.016	0.013

According to the mentioned results, a trade-off among the different errors is produced by adopting the following parameters (coded values in brackets):  $a_p = 0.066$  mm (-1),  $a_e = 0.2$  mm (-1) and  $f_z = 12.5$   $\mu\text{m}/\text{rev}$  tooth (-1). With this configuration only minimal Taper, Banana and Bell residual errors are produced. Figure 3 depicts Test #42 that adopted these parameters combination.

All of these results are useful criteria to choose the correct parameters combination to obtain the best pin geometrical quality in case of high AR pin micromilling.

Although in this case it is possible to outline the best parameters set to reduce the geometrical deviations, an optimization routine, such as the *Response Surface Methodology* (RSM) [20] or the *Kriging Method* [25], have to be performed to minimize the effects of the *Chebyshev* coefficients through on multi-objective optimization routine.

**Table 6: Plot analysis of the ANOVA for  $T_0$  and  $T_1$  (Table 5)**

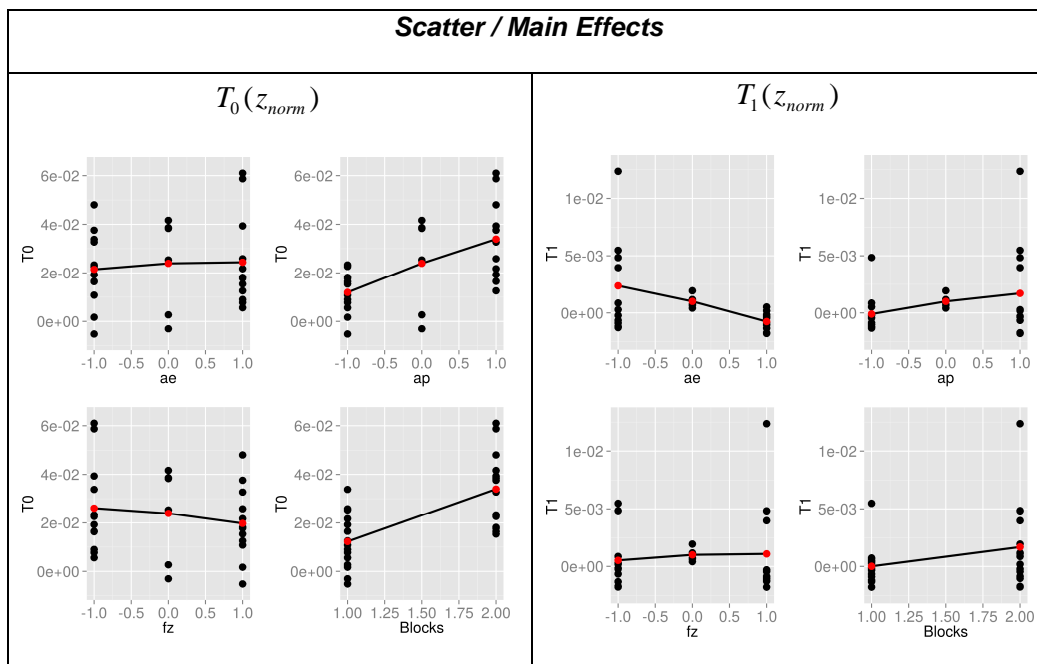

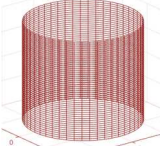


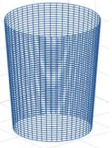


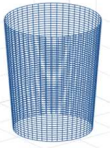






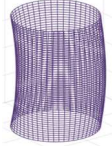





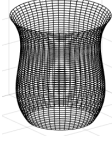
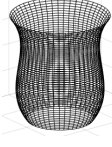

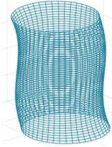
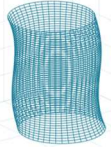





Table 7: Effect of the cutting parameters on the geometrical deviation

Chebychev coefficients	$a_p$		$a_e$		$f_z$	
	-1	1	-1	1	-1	1
T0						
T1						
T2						
T2 sin						
T3						
T3 sin						



## 5. Feasibility assessment of indirect geometrical monitoring

Cutting forces, generated from the interaction between the cutting tool and the part, reveal information about the involved cutting mechanism, the actual tool engagement, the machine and tool state (e.g. wear state, geometric runout, vibrations etc.) and then represent a fruitful source for implementing process monitoring and diagnostic methods.

This paragraph discusses the link between the acquired cutting forces and the final micropin geometrical errors in order to understand the feasibility of implementing an online geometry monitoring.

### 5.1. Cutting Force Map Computation

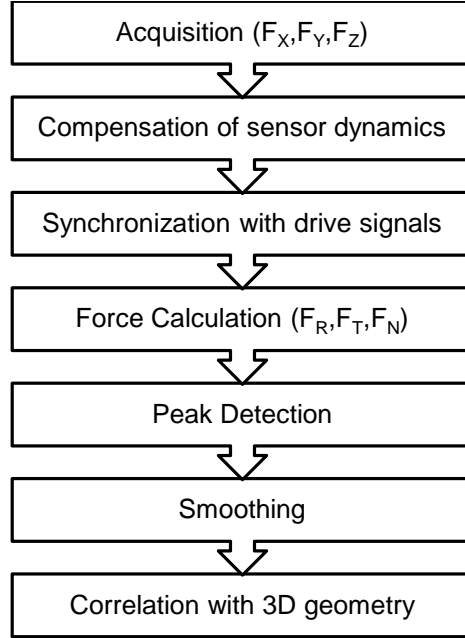
Different phenomena affect cutting forces generated in pin micromilling. In general, assuming the material properties as homogeneous, the tool wear as negligible, and no variations of the machine cutting parameters along the toolpath, no changes in the generated cutting forces along the tool trajectory are expected. Conversely, the presence of systematic force variations could reveal machining errors or unexpected behavior of cutting tool process. The high flexural stiffness, characterizing the raw pin geometry, varies exponentially with the pin height and changes considerably due to the stock removal producing a time-changing system dynamics. The adopted top-down helicoidal toolpath is such that the contact between tool and force varies along Z direction in a continuous way thus increasing the possibility to develop a taper error along the pin axis.

To evaluate these effects as 3D-Force Map, as discussed in [11] is synthesized for each pin, following the procedure showed in Figure 7.

This map, showing the cutting forces behavior along the entire toolpath, is correlated to the final geometry to verify whether some relationships can be extracted.

After the cutting forces acquisition, the sensor inertial response is filtered out from the signals through an inverse dynamic filtering approach. In this approach, each element of the force vector spectrum is simply divided by the corresponding element of the model which is constituted by the Frequency Response Function of the dynamometer in X and Y direction. Differently to the macromilling case showed in [11], this aspect has to be mandatorily addressed in micromilling force analysis, where the high rotational speeds introduces high frequency force components. The sensor response functions are computed by performing an impact test on the force measurement system. The system response was characterized five times for different manual operations of pin fixture and a highly repetitive response was noticed with no significant variations among the replicates. The lowest resonance frequencies of the fixturing are

about at 4000 Hz in both X and Y directions. The application of the compensation scheme results mandatory to reduce the strong dynamic amplification given by these contributes and affecting the measured force.



**Figure 7: Procedure to generate the 3D cutting Force Map**

The force readings are then synchronized with the drive signals coming from the numerical controller of the machine (NC) by means of the digital trigger signals acquired for that purpose. The lag in the synchronization equal at maximum 1.8 ms, i.e. the discrete time step of the NC signals.

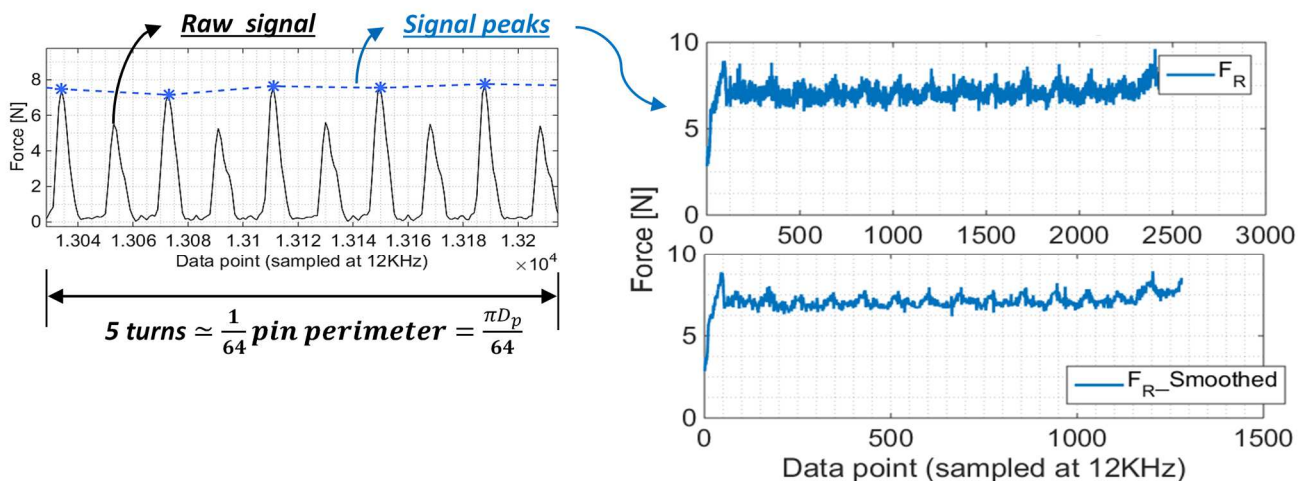
Since the tool is rotating around the pin axis whilst the dynamometer is fixed, the tangential, normal and resultant cutting forces seen by the pin ( $F_R$ ,  $F_N$ ,  $F_T$ , respectively in Eq. 6,7,8), are computed starting from the acquired X-Y-Z signals. This can be achieved by extracting  $\beta$ , i.e. the angular position of the tool in respect to the center of the pin, from the drive signals and by computing the following formulas:

$$F_R = \sqrt{F_X^2 + F_Y^2} \quad \text{Eq. (6)}$$

$$F_N = F_X \cdot \cos \beta + F_Y \cdot \sin \beta \quad \text{Eq. (7)}$$

$$F_T = -F_X \cdot \sin \beta + F_Y \cdot \cos \beta \quad \text{Eq. (8)}$$

The modulus and directions of the abovementioned force components affect the instantaneous radial deflection of the pins. Since these signals are strictly dependent from the instantaneous cutter engagement arc, their typically cosinusoidal behavior is synthetized by only considering the local force maxima, as synthetic force indicators. A peak detection algorithm is used to find out the local force maxima from the raw data vectors. Due to the effect of the geometric runout of the end-mill, alternating force maxima can be noticed in Figure 8, confirming that the two tool cutters approach in a different way the metal chip. Negligible variations along the tool trajectory are shown in the signals and therefore the only local maxima of the overexposed cutter, are selected (blue asterisk markers in Figure 8). To conclude the preparation of the cutting Force Map a smoothing function is applied on the force vectors to enable the calculation of a correlation index with the geometry data cloud. After a sensitivity analysis that confirmed small influence on the results, the two sources are downsampled to generate an arbitrary value of 64 points per revolution by adopting a smoothing average filter. Figure 9 shows the force maxima before and after the application of the smoothing filter during test #1.



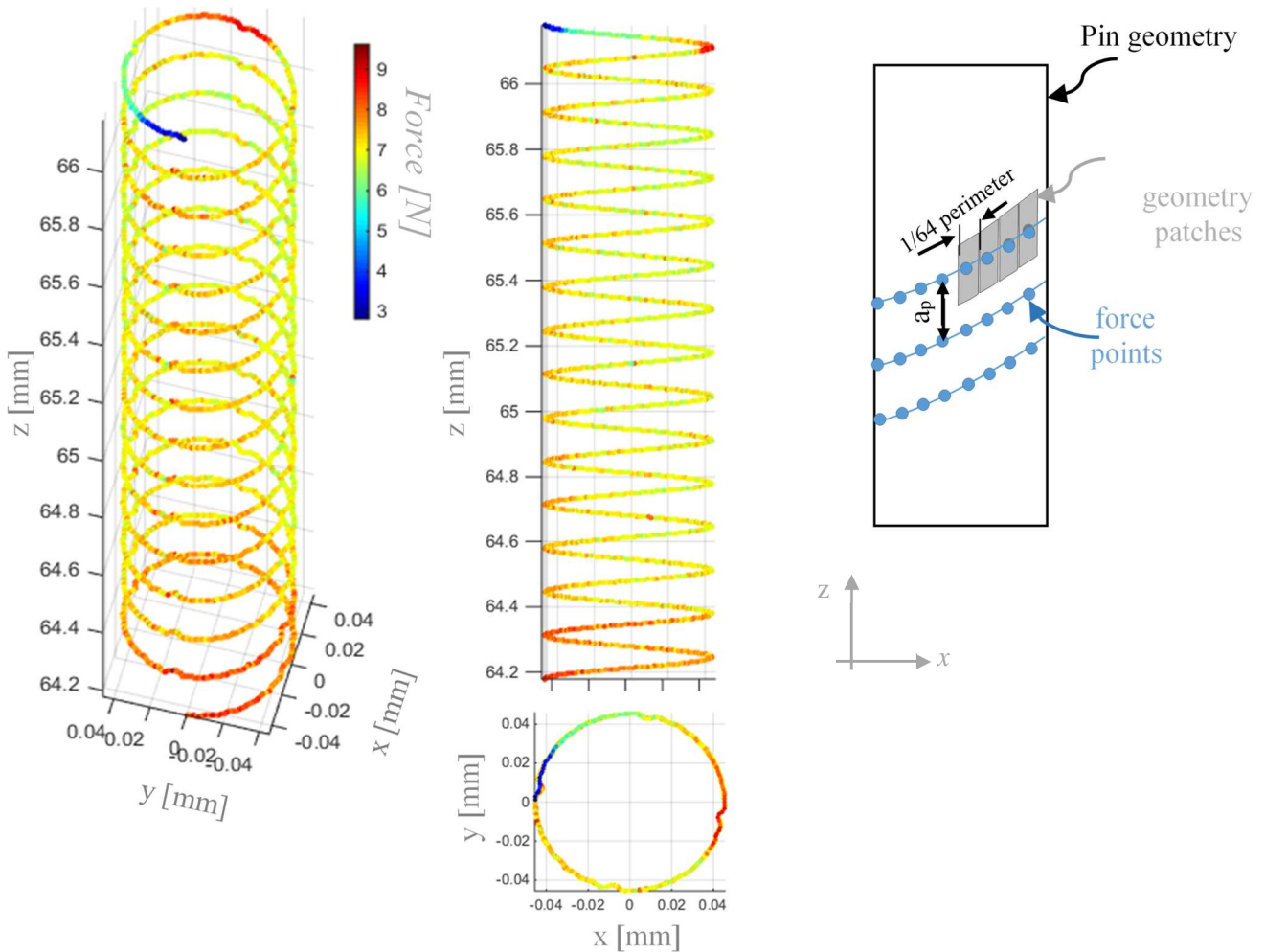
**Figure 8: Peak detection (A) and Smoothing on cutting forces maxima (B) during test #1**

## 5.2. Correlation between cutting Force Map and geometrical errors

Due to the lack of information related with the original angular position of the pin inside the milling machine, the correlation between the data referring to the forces and to the actual pin geometry depends on the orientation phase between the two data clouds. To cope with this limit, the correlation index is computed for variable phase shifts (steps of  $1^\circ$  are adopted), and a correlation vector is obtained for each pin.

The final correlation index between the two grids is represented by the maximum modulus of this vector (a period behavior every  $\pi$  is in any case showed).

In total twenty-five *downmilling* cutting tests (out of total thirty tests) are analyzed since *upmilling* tests, as above discussed, failed. Cutting force acquisitions of five tests were corrupted by electrical disturbance and therefore were not taken into account.



**Figure 9: 3D cutting Force Map: smoothed  $F_R$  maxima during test #1 (A); geometry patches used for computing the correlation (B)**

Figure 10 shows the maximum correlations between the force components values and the mean radius of the pin, in the investigated angular shift range. There is a certain similarity among the cutting force components in the sense that correlation is similar in magnitude for all three of them in all the different cutting tests. A correlation larger than -0.6 is noticeable for pin #27 and values bigger than 0.3 appear for eight different tests (#20, #21, #24 #25 #41, #42, #45,

#46). However, the remaining sixteen tests produced negligible correlations in the range of  $\pm 0.2$  that reveal a lack of direct connection between the process forces and the achieved final pin geometry.



Figure 10: Correlation index between  $F_R$ ,  $F_T$ ,  $F_N$  and geometry of the pin

## 6. Discussion and Conclusion

An analysis regarding the effect of process parameters on the geometrical accuracy of high aspect ratio micromilled steel pins, with nominal diameter equal to  $100 \mu\text{m}$ , is presented. The adopted helicoidal interpolation is used varying the axial depth of cut  $a_p$ , radial depth of cut  $a_e$ , feed per tooth  $f_z$  and milling strategy (*upmilling* and *downmilling*). The geometrical error deviations were extracted from the microscope 3D point cloud: they consisted in the inclination angle of the pin in respect to the pin base and in independent error mode-shapes (i.e. Diameter scale, Taper, Barrel, Banana, Bell, S-Shape) extracted from the application of a *Chebyshev* fitting algorithms on the data.

The first results is that *upmilling* strategy has to be avoided when dealing with high aspect ratio pin machining. On one side, this is in agreement with best-practice rules provided by tool manufacturers and “mold-die” operators that suggest *downmilling* for increasing parts surface finish limiting tool wear. On the other side, this result shows some contrast with previous results regarding thin wall micromilling that indicates *upmilling* as the best machining conditions for thin walls [13]. This extreme effect played by the cutting configuration on the machinability of high aspect ratio steel components is worthy of note and the attention goes to the implications that large ploughing effects in conjunction with high static compliance of either parts or tools, have on the final part accuracy.

Another finding is that most of the pins machined with *downmilling* strategy resulted smaller in the average diameter. On one hand, tool diameter measurements accuracy is essential for achieving correct pin diameter. Additional systematic deviations of the pin diameter are caused by the under cutting phenomenon related to the low part/mill rigidity: this aspect is not easily predictable during the process setup. On the other side, the systematic diameter variation opens the possibility to implement compensation schemes on the average pin diameter during the process setup for increase process accuracy.

Moreover, by looking at all the others relevant geometrical deviations of the pins, it emerges that they are systematically affected by the cutting parameters; their selection then represents a critical step in the designing of the entire manufacturing cycle of the pins and of their functionalities.

The developed methodology, based on the application of a *Chebyshev* fitting, resulted suitable for analyzing the geometrical deviations of pin micro-features thus allowing the identification of the link between them and the original error sources, in terms of process parameters. Through this approach, it is possible to define optimal sets of micromilling parameters for minimization of each classical “cylindricity error shape”, considering the requirements and the final functionality of the pins.

The method can be used for describing the cilindricity errors and link them with process parameters, in many other machining and manufacturing processes both in macro and micro scale, such as deep holes drilling, turning and grinding of cylindrical components and Additive Manufacturing products. The main limitation is the capacity to describe only simple error shapes, whilst more complexity such as surfaces with sharp changes or discontinuities would require the use of functions with higher order terms. The complexity of the method is justified by its capacity to cope with processes that involves several control variables, whose relationships with the achieved geometrical accuracy cannot be easily predicted with other methods.

This paper demonstrates the application of this method for studying the geometrical variations of a microfeature in relation to the machining parameters adopted. The study allowed pointing out the selection rules of the process parameters basing on the reduction of the pins geometrical deviations. The axial depth of cut and its interactions with the other cutting parameters resulted the most significant parameter for minimizing the geometrical deviations, in particular the scale and the taper errors. In this case, lower values of axial depth of cut guaranteed lower errors values.

Despite there is a huge importance of the feed per tooth for the micromilling removal mechanism, in relation to the Minimum Chip Thickness effect, this parameter showed a limited effect on the final part geometrical deviations.

Additionally, particular importance of the roughing milling tool, used for generating the semi-finished pins, was showed. The evidence that the final pin geometry is generated not only by finishing operation poses the attention on the importance of each step of the manufacturing cycle, which therefore must be adequately designed. Eventually, this study pointed out that the cutting forces in high aspect ratio pin micromilling are not significantly correlated (in terms of linear correlation) with the final geometrical deviations of the parts; the complex interaction between the high compliant part and tool generated in micromilling is such that the generated forces are not directly linkable with the instantaneous material removed. This fact prevents the possibility to exploit the force prediction methods available in literature and to implement indirect geometrical monitoring schemes. There is still the need, for the moment, to perform time-expensive post-process measurements to qualify the accuracy of micromilled pins. Future developments of the presented research will test the obtained results on different pin shapes, materials and dimensions. This will foster the application of the approach in real industrial microapplications in the mold-die and microextrusion industry where pin geometry characteristics, as well as their surface finishing quality, are important for the final functionality of the products.

## 7. Acknowledgements

The authors are very grateful to Eng. Cacciatore and Eng. Conca for their valuable support to the presented research. This study has been partly founded by the European Union Seventh Framework Programme FP7/2007-2013, under grant agreement n° 285075 (MuProD).

LP gratefully acknowledge the UKs Engineering and Physical Sciences Research Council (EPSRC) founding of the EPSRC Fellowship in Manufacturing: Controlling Variability of Products for Manufacturing (Ref:EP/K037374/1).

## 8. References

- [1] Gietzelt T, Eichorn L, Schubert K, Manufacturing of microstructures with high aspect ratio by micromachining, *Microsyst Technol* 2008; 14:1525-1529.
- [2] Masuzawa T, State of the art of micromachining, *CIRP Annals - Manufacturing Technology* 2000; 49: 473-488.
- [3] Dornfeld D, Min S, Takeuchi Y, Recent advances in mechanical micromachining, *CIRP Annals - Manufacturing Technology* 2006; 5:745-768.

- [4] Huang Y, Zhang X, Xiong Y, Finite Element Analysis of Machining Thin-Wall Parts: Error Prediction and Stability Analysis, Finite Element Analysis – Applications in Mechanical Engineering, Publisher: InTech, 2012, ISBN 978-953-51-0717-0, 392 pages, DOI: 10.5772/3249
- [5] Bolsunovskiy S, Vermel V, Gubanov G, Kacharava I, Kudryashov A, Thin-Walled Part Machining Process Parameters Optimization based on Finite-Element Modeling of Workpiece Vibrations, 14th CIRP Conference on Modeling of Machining Operations (CIRP CMMO); 2013, 8:276–280.
- [6] Bang YB, Lee KM, Oh S, 5-axis micromilling machine for machining micro parts, International Journal of Advanced Manufacturing Technology 2005; 25:888–894.
- [7] Bordatchev EV, Tauhiduzzaman M, Kugler T, Katz A, Bohr R, Demonstration of advanced capabilities of 5-axis micromilling: geometries with high-aspect ratio and/or optical surface quality, ICOMM 2013 - 8th International Conference on MicroManufacturing, Victoria (Canada) 2013; 357-362.
- [8] Annoni M, Rebaioli L., Semeraro Q, Thin wall geometrical quality improvement in micromilling, International Journal of Advanced Manufacturing Technology 2015; 79:881-895.
- [9] Annoni M, Colosimo BM, Pagani L, Rebaioli L, Semeraro Q, Geometrical quality improvement of high aspect ratio micromilled pins, Transactions of the North American Manufacturing Research Institution of SME 2014; 42.
- [10] Benardos PG, Mosialos S, Vosniakos GC, Prediction of workpiece elastic deflections under cutting forces in turning, Robotics and Computer-Integrated Manufacturing 2006; 22:505-514.
- [11] Lopez de Lacalle LN, Lamikiz A, Sanchez JA, Fernandez de Bustos I, Recording of real cutting forces along the milling of complex parts, Mechatronics 2006; 16:21-32.
- [12] Marsh ER, Moerlein AW, Deakyne TRS, Van Doren MJ, In-process measurement of form error and force in cylindrical-plunge grinding, Precision Engineering 2008; 32: 348-352.
- [13] Li P, Zdebski D, Langen HH, Hoogstrate AM, Oosterling JAJ, Schmidt RHM, Allen DM, Micromilling of thin ribs with high aspect ratios, J Micromech Microeng. 2010; 20:115013.
- [14] Liu X, Devor RE, Kapoor SG, An analytical model for the prediction of minimum chip thickness in micromachining, Journal of Manufacturing Science and Engineering 2006; 128: 474-481.
- [15] Jemielniak K, Arrazola PJ, Application of AE and cutting force signals in tool condition monitoring in micro-milling, CIRP Journal of Manufacturing Science and Technology 2008; 1:97-102.



- [16] Rusu RD, Cousins S, 3D is here: Point Cloud Library (PCL), IEEE International Conference on Robotics and Automation (ICRA) 2011.
- [17] Fischler MA, Bolles RC, Random Sample Consensus: A paradigm for model fitting with applications to image analysis and automated Cartography, Communications of the ACM 1981; 24:381-395.
- [18] Venables WN, Ripley BD, Modern Applied Statistics with S, Springer, 2002, 498 Pages, DOI: 10.1007/978-0-387-21706-2.
- [19] Johnson RA, Wichern DW, Applied Multivariate Statistical Analysis, Prentice-Hall Inc, 1988:AMS:59551, ISBN 0130411469, Upper Saddle River, NJ, USA.
- [20] Montgomery Douglas C, Design and Analysis of Experiments, John Wiley & Sons, 2006:DAE:1206386, ISBN 0470088109.
- [21] Colosimo BM, Pacella M, Analysing the effect of process parameters on the shape of 3D profiles, Journal of Quality Technology 2011; 43.
- [22] ISO 12780-1:2011, Geometrical product specifications (GPS) – Straightness – Part 1: Vocabulary and parameters of straightness.
- [23] Colosimo BM, Pacella M, Semeraro Q, Statistical process control for geometric specifications: on the monitoring of roundness profiles, Journal of Quality Technology 2008; 40:1-18.
- [24] Henke RP, Summerhaysb KD, Baldwin JM, Cassoub RM, Brownd CW, Methods for evaluation of systematic geometric deviations in machined parts and their relationships to process variables, Precision Engineering 1999; 23(4):273-292
- [25] Donald RJ, Schonlau M, Welch WJ, Efficient Global Optimization of Expensive Black-Box Functions, Journal of Global Optimization 1998; 13:455-492

## Appendix A

Due to the high cutting speed the tool trajectories can be assumed as translated circles and therefore the engagement angle of the tool  $\varphi_t$  can be calculated as:

$$\varphi_t = \arccos\left(\frac{R_t - a_{eff}}{R_t}\right) \quad \text{Eq. (9)}$$

where the effective radial depth of cut  $a_{eff}$ , generating the actual contact arc between the tool and the workpiece, is:

$$a_{eff} = \frac{a_e \left(1 + \frac{a_e}{2R_p}\right)}{1 + \frac{R_t}{R_p}} \quad \text{Eq. (10)}$$

Therefore, the maximum nominal chip thickness  $h_{n\_max}$ , reached at the end of the contact arc, can be approximated as:

$$h_{n\_max} = P_{cut} \cos(\varphi_t - \varphi_{ae}) \quad \text{Eq. (11)}$$

where:

$$P_{cut} = (R_p + a_e) \cdot \varphi_{cut} \quad \text{Eq. (12)}$$

The angle  $\varphi_{cut}$  is between the trajectories of two subsequent cutters (determined by the machining feed) whilst  $\varphi_{ae}$  is the angle between the Pin Centre Point ( $PCPradius(i)$ ) and the centre-to-centre connection line between pin and tool in Figure 2.  $\varphi_{ae}$  can be easily estimated from kinematic equations with a symbolic equation solver.

## Appendix B

**Table 8: Executed Experimental plan**

<b>Run Order</b>	<b>Blocks</b>	<b><math>a_p</math></b>	<b><math>a_e</math></b>	<b><math>f_z</math></b>	<b>Strategy</b>
1	2	0	0	0	downmilling
2	2	1	-1	1	upmilling
3	2	-1	1	1	upmilling
4	2	0	0	0	upmilling
5	2	-1	-1	-1	upmilling
6	2	1	1	-1	upmilling
7	2	0	0	0	downmilling
8	2	1	-1	1	upmilling
31	2	1	-1	-1	upmilling
32	2	-1	1	-1	upmilling
33	2	-1	-1	1	upmilling
34	2	1	1	-1	downmilling
35	2	-1	-1	-1	downmilling
36	2	1	1	1	upmilling
37	2	1	-1	-1	upmilling
38	2	1	-1	1	downmilling

<b>9</b>	2	-1	1	1	<i>upmilling</i>
<b>10</b>	2	0	0	0	<i>upmilling</i>
<b>11</b>	2	-1	-1	-1	<i>upmilling</i>
<b>12</b>	2	1	1	-1	<i>upmilling</i>
<b>13</b>	1	-1	-1	1	<i>downmilling</i>
<b>14</b>	1	1	-1	1	<i>upmilling</i>
<b>15</b>	1	1	1	1	<i>downmilling</i>
<b>16</b>	1	-1	1	1	<i>upmilling</i>
<b>17</b>	1	-1	1	-1	<i>downmilling</i>
<b>18</b>	1	-1	1	-1	<i>downmilling</i>
<b>19</b>	1	-1	-1	1	<i>downmilling</i>
<b>20</b>	1	-1	1	-1	<i>downmilling</i>
<b>21</b>	1	1	-1	-1	<i>downmilling</i>
<b>22</b>	1	1	1	1	<i>downmilling</i>
<b>23</b>	1	1	-1	-1	<i>downmilling</i>
<b>24</b>	1	0	0	0	<i>downmilling</i>
<b>25</b>	1	0	0	0	<i>upmilling</i>
<b>26</b>	1	-1	-1	1	<i>downmilling</i>
<b>27</b>	1	1	-1	-1	<i>downmilling</i>
<b>28</b>	1	1	1	-1	<i>upmilling</i>
<b>29</b>	1	1	1	1	<i>downmilling</i>
<b>30</b>	1	-1	-1	-1	<i>upmilling</i>

<b>39</b>	2	-1	1	1	<i>downmilling</i>
<b>40</b>	2	-1	1	-1	<i>upmilling</i>
<b>41</b>	2	1	-1	1	<i>downmilling</i>
<b>42</b>	2	-1	-1	-1	<i>downmilling</i>
<b>43</b>	2	1	1	-1	<i>downmilling</i>
<b>44</b>	2	-1	1	1	<i>downmilling</i>
<b>45</b>	2	1	1	-1	<i>downmilling</i>
<b>46</b>	2	-1	-1	-1	<i>downmilling</i>
<b>47</b>	2	1	-1	1	<i>downmilling</i>
<b>48</b>	2	1	-1	-1	<i>upmilling</i>
<b>49</b>	2	0	0	0	<i>downmilling</i>
<b>50</b>	2	-1	1	1	<i>downmilling</i>
<b>51</b>	2	-1	-1	1	<i>upmilling</i>
<b>52</b>	2	0	0	0	<i>downmilling</i>
<b>53</b>	2	0	0	0	<i>upmilling</i>
<b>54</b>	2	0	0	0	<i>downmilling</i>
<b>55</b>	2	0	0	0	<i>upmilling</i>
<b>56</b>	2	-1	1	-1	<i>upmilling</i>
<b>57</b>	2	1	1	1	<i>upmilling</i>
<b>58</b>	2	-1	-1	1	<i>upmilling</i>
<b>59</b>	2	1	1	1	<i>upmilling</i>
<b>60</b>	2	0	0	0	<i>upmilling</i>